Impact of negative triangularity on edge plasma transport and turbulence in TOKAM3X simulations

E. Laribi, E. Serre, P. Tamain, H. Yang

Impact of negative triangularity on edge plasma transport and turbulence in TOKAM3X simulations

E. Laribi[b], E. Serre[a,*], P. Tamain[b], H. Yang[a]

[a] *Aix-Marseille Univ., CNRS, Centrale Marseille, M2P2 Marseille, France*
[b] *IRFM, CEA Cadarache, F-13108 St. Paul-lez-Durance, France*

Abstract

The impact of triangularity on edge plasma transport and turbulence is addressed from full 3D turbulence simulations performed with TOKAM3X. Flux driven fluid simulations are run on analytical magnetic equilibria generated with positive and negative triangularity δ in a bottom limiter configuration. The conservation of the energy is assured by the increase of the bottom limiter radial position from $\delta > 0$ to $\delta < 0$. Changing the triangularity impacts both the plasma equilibrium and the turbulence. In particular, negative triangularity leads to a reduction of the density and electron temperature decay lengths in agreement with the literature. Concerning the turbulence, in all the simulations, it remains ballooned with an enhanced level of fluctuations at low field side in comparison to the high field one. Moreover, no clear trend is visible on the relative level of fluctuations of both density and electron temperature in the CFR whereas an enhancement (resp. reduction) is visible in the scrape-off layer at the low field side midplane for the negative (resp. positive) triangularity simulations. This behaviour differs from TCV and DIII-D measurements which show the benefit of negative triangularity in terms of turbulence reduction and increased confinement. However, no conclusion is drawn from our preliminary study concerning the impact of triangularity on the turbulent transport. Change in triangularity impacts many simulation control parameters, as in the experiments, and that the analysis of its impact alone on the dynamics of the plasma is not obvious in this configuration.

Keywords: Negative triangularity, tokamak simulation, edge plasma, scrape-off layer, turbulence

*Corresponding author
Email address: eric.serre@univ-amu.fr (E. Serre)

Introduction

The success of future fusion devices as ITER is conditional on the access to long enough energy confinement time and high enough pressure of the plasma. Recently, experiments realised on TCV and DIII-D machines of negative triangularity plasma shapes have revealed the possibility to reach global confinement levels (in terms of τ_e and β) in free-ELMs L-mode similar to H-mode ones [1, 2, 22, 24]. Thus, negative triangularity could provide an elegant solution for power plant design, the plasma being able to be heated to reactor relevant conditions without the potential critical damages caused by ELMs. These observations have motivated the fusion community to intensify both the modelling and the experimental efforts on the impact of negative triangularity on global confinement and power exhaust. Concerning global confinement, two decades of experiments realised on TCV have shown that negative triangularity leads to a substantial reduction of the fluctuations consistent with the beneficial effect observed on energy confinement [4, 5, 10, 22, 24]. Gyrokinetic simulations (GENE [8, 24], GS2 [9], LORB5[10, 22]) have been able to reproduce qualitatively the results concerning the reduction of electron heat transport with negative triangularity. In particular, these simulations have shown that this reduction was linked, at least partly, to the stabilizing influence of negative triangularity on the trapped electron mode (TEM). In contrast, concerning the impact of triangularity on the power exhaust problematic, very few studies have been carried out despite its fundamental importance for tokamak viability. One of them concerns the impact of upper triangularity δ_{up} on scrape-off layer power fall-off length λ_q in a divertor configuration in TCV [11]. The authors report smaller λ_q^{out} measured at the outer divertor target for decreasing δ_{up} together with higher edge temperature $T_{e,edge}$ leading to increased confinement. In opposition, the power fall-off length at the inner divertor target λ_q^{inn} has a non-monotonic behaviour with changing triangularity. More recently, the effect of shaping including negative triangularity on the scrape-off layer plasma has been investigated in TCV high field limited plasmas and by the 3D turbulent fluid code GBS [6, 7]. Both the fluid code and the experimental measurements revealed the steepening of the averaged gradients at low field side midplane in the scrape-off layer. Up to now, to our knowledge, no other studies have been realised on the impact of negative triangularity on the scrape-off layer plasma. Hence, there is a strong demand for both experiments and modelling on this challenging question. The shaping capabilities of the edge plasma fluid code

TOKAM3X [12, 13] provide the opportunity to investigate in a systematic way the triangularity effects on the edge plasma. The fluid edge electrostatic 3D code TOKAM3X includes the physics suspected to play a significant role in the particle and energy transport in the edge plasma (diffusion, mean drifts convection, turbulence triggered by electrostatic interchange and electrostatic resistive drift waves) in arbitrary axisymmetric magnetic geometry. In this contribution, we propose to study the impact of analytical negative triangularity magnetic equilibria on both the edge closed field lines region (CFR) and the scrape-off layer (SOL) plasma in a bottom limited configuration. For this purpose, five triangularities are investigated $\delta = -0.5, -0.3, 0.0, +0.3$ and $+0.5$.

The following contribution is divided in 3 parts. The TOKAM3X physical model, parameters and magnetic geometries used for these numerical simulations is exposed in section 1. In section 2, the impact of triangularity on time averaged radial profiles at low field side midplane and on targets heat flux distribution are discussed. In parallel, the modifications of the turbulence characteristics with triangularity are exposed. Finally, the comparison with other numerical scans and experiments in section 3 will enable to identify whether or not the physical phenomena described by the TOKAM3X model are sufficient to understand and reproduce the impact of triangularity in the CFR and in the SOL plasma.

1. TOKAM3X simulations setup

In this section, the physical model of the TOKAM3X code and the values of the parameters chosen for this scan are exposed.

1.1. Physical model

TOKAM3X is a 3D turbulent fluid code of the edge plasma that can treat arbitrary toroidal axisymmetric magnetic configurations. It solves the electrostatic 3D drift-reduced Braginskii equations under the quasi-neutrality assumption [13]. The code models the dynamics of six fields: the density N, the parallel ion momentum $\Gamma = Nu^i_\parallel$ where $u^i_\parallel$ is the parallel to $\mathbf{B}$ component of ion velocity $\mathbf{u^i}$, the electrostatic potential Φ, the plasma parallel electric current $j_\parallel$, the electron and ion temperatures T_e, T_i after the resolution of the particle balance equation (1), the parallel ion momentum conservation equation (2), the parallel ohms law (from parallel electron momentum conservation neglecting electron mass) (3), the charge conservation equation (4), the electron energy $E_e = \frac{3}{2}NT_e$ conservation

equation (5) and finally, the ion energy $E_i = \frac{\Gamma_i^2}{2N} + \frac{3}{2}NT_i$ conservation equation (6).

$$\partial_t N + \nabla \cdot (N(\mathbf{u}_{||}^{\mathbf{i}} + \mathbf{u}_{\perp}^{\mathbf{i}})) = S_N + \nabla \cdot (D_{\perp N} \nabla_{\perp} N) \tag{1}$$

$$\partial_t \Gamma + \nabla \cdot (\Gamma(\mathbf{u}_{||}^{\mathbf{i}} + \mathbf{u}_{\perp}^{\mathbf{i}})) = -\nabla(P) + \nabla \cdot (\mathbf{u}_{||}^{\mathbf{i}} D_{\perp N} \nabla_{\perp} N + D_{\perp \Gamma} N \nabla_{\perp} \mathbf{u}_{||}^{\mathbf{i}}) \tag{2}$$

$$\eta_{||} N j_{||} = \nabla_{||}(P_e) - N \nabla_{||}(\Phi) + 0.71 N \nabla_{||}(T_e) \tag{3}$$

$$\partial_t W + \nabla \cdot (W(\mathbf{u}_{||}^{\mathbf{i}} + \mathbf{u}_{\perp}^{\mathbf{i}})) = \nabla \cdot (D_{\perp W} \nabla_{\perp} W) + \nabla \cdot (N(\mathbf{u}_{\nabla}^{\mathbf{i}} - \mathbf{u}_{\nabla \mathbf{B}}^{\mathbf{e}})) + \nabla \cdot (\mathbf{j}_{||}) \tag{4}$$

$$\begin{aligned} &\partial_t E_e + \nabla \cdot ((E_e + P_e)\mathbf{u}_{||}^{\mathbf{i}} + E_e \mathbf{u}_{\perp}^{\mathbf{e}}) = S_{E_e} + \nabla \cdot (\kappa_0^e T_e^{\frac{5}{2}} \nabla_{||}(T_e \mathbf{b})) \\ &-P_e \nabla \cdot (\mathbf{u}_{\perp}^{\mathbf{e}}) + \frac{\Gamma}{N} \nabla_{||}(P_e) + Q^e + \nabla \cdot (D_{\perp N} \frac{3}{2} T_e \nabla_{\perp} N + D_{\perp T_e} N \nabla_{\perp} T_e) \end{aligned} \tag{5}$$

$$\begin{aligned} &\partial_t E_i + \nabla \cdot ((E_i + P_i)\mathbf{u}_{||}^{\mathbf{i}} + E_i \mathbf{u}_{\perp}^{\mathbf{i}}) = S_{E_i} + \nabla \cdot (\kappa_0^i T_i^{\frac{5}{2}} \nabla_{||}(T_i \mathbf{b})) - P_i \nabla \cdot (\mathbf{u}_{\perp}^{\mathbf{i}}) \\ &-\frac{\Gamma}{N} \nabla_{||}(P_e) + Q^i + \nabla \cdot (D_{\perp T_i} N \nabla_{\perp} T_i) + \nabla \cdot (D_{\perp N} (\frac{3}{2} T_i + \frac{\Gamma^2}{2N}) \nabla_{\perp} N + D_{\perp \Gamma} \Gamma \nabla_{\perp} \mathbf{u}_{||}^{\mathbf{i}}) \end{aligned} \tag{6}$$

In all the equations, $||$ and $\perp$ represent respectively the parallel and the perpendicular to B component of any vector. $P = P_e + P_i$ is the total pressure of the plasma. $W = \nabla \cdot (\frac{1}{B^2} \nabla_{\perp} \cdot \Phi + \frac{1}{NB^2} \nabla_{\perp} \cdot P_i)$ is what is called generalized vorticity of the plasma. $Q^{e,i}$ is a friction energy transfer term between ions and electrons due to collisions. S_{N,E_e,E_i} are the source terms for particles and energies. The drift approximation ($\omega \ll \omega_{ci}$, $\rho_L \ll l$) gives the expression of the first order perpendicular velocities from the conservation equations of the perpendicular momentum for each species:

$$\mathbf{u}_{\perp}^{i} = \mathbf{u}_{E \times B} + \mathbf{u}_{\nabla p \times B}^{i} \qquad\qquad \mathbf{u}_{\perp}^{e} = \mathbf{u}_{E \times B} + \mathbf{u}_{\nabla p \times B}^{e}$$

The Braginskii closure [14] terms compensate diamagnetic drift advection terms leaving only the contribution of the magnetic drift (diamagnetic cancellation). This allows us to replace the diamagnetic drift by the magnetic drift wherever advection by the diamagnetic velocity appears in the fluid drift equations. In the code, all quantities are normalized with respect to a reference density n_0, temperature T_0 (the same for ion and electron), and the magnetic field B_0. Spatial quantities are normalized to the Larmor radius $\rho_L = \frac{\sqrt{m_i T_0}}{eB_0}$ (where m_i is the ion mass, and e the elementary charge), and time to the ion cyclotron period $\frac{2\pi m_i}{eB_0}$. As a consequence, the electric potential ϕ and the parallel velocity $u_{||}^i$ are, respectively, normalized to T_0/e and $\sqrt{\frac{2T_0}{m_i}}$.

Moreover, the diffusive terms, not included in Braginskii equations, are added to the balance equations. Such terms represent dissipation mechanisms at scales smaller than the mesh grid, thus not modelled self-consistently. They are mandatory for the numerical stability of the code. Under this normalization, the cross-field diffusion coefficients $D_{\perp,F}$ for each field $F = N, \Gamma, W, T_e, T_i$ are fixed to $D_{\perp,F} = 1 \times 10^{-2}$ (a.u.) given the chosen normalization. The parallel resistivity and the coefficients of parallel conduction for electrons and ions of the plasma are treated self consistently with their electron and ion temperatures dependence as follow:

$$\eta_{\parallel} = 0.51 \nu_* \frac{m_e Z^2 ln(\Lambda)}{m_i T_e^{3/2}} \qquad \kappa^e_{0\parallel} = \frac{3.16}{\nu_*} \frac{m_i T_e^{5/2}}{m_e Z^2 ln(\Lambda)} \qquad \kappa^i_{0\parallel} = \frac{3.9}{\nu_*} \sqrt{\frac{2m_i}{m_e}} \frac{T_i^{5/2}}{Z^4 ln(\Lambda)}$$

Where $\frac{m_i}{m_e}$ the ratio between ion and electron mass is fixed to 2723 and the ion charge number Z to 1 to consider a deuterium plasma relevant for fusion reactors, T_e and T_i are the electronic and ionic temperatures respectively, $ln(\Lambda)$ is the coulomb logarithm fixed to 10 and ν_* is the collisionality of the plasma. Under the normalization chosen, the collisonnality is fixed to $\nu_* = 5 \times 10^{-2}$ (a.u.), whereas the typical value in a medium size Tokamak is about 1×10^{-2} (a.u.), thus smaller than the parameter retained here. This choice is due to numerical cost considerations.

TOKAM3X is able to model both the edge closed field lines region (CFR) and the scrape-off layer (SOL) open field lines region. Moreover, the code is flux driven, i.e. the total amount of particles and energy are forced by volumic sources S_N and $S_{E_{e/i}}$ respectively. An important source of particles will not be taken into account in our simulations: neutral recycling. To take into account neutrals dynamics in the SOL, TOKAM3X can be coupled to EIRENE module [17]. However, as a first step, this paper focus on the study of the impact of triangularity independently from neutrals dynamics.

Boundary conditions on the limiter are given by the Bohm-Chodura derivation for the ionic velocity, parallel electric current and parallel heat flux reaching the sheath [13, 16].

$$|\mathbf{u^i} \cdot \mathbf{n}_{target}| \geq c_s |\mathbf{b} \cdot \mathbf{n}_{target}|$$
$$j_{\parallel} = \Gamma \left(1 - e^{\frac{\Lambda - \Phi}{T_e}}\right)$$

$$\vec{q}_e \cdot \vec{n}_{target} = \gamma_e T_e N \vec{u}_i \cdot \vec{n}_{target} \qquad \vec{q}_i \cdot \vec{n}_{target} = \gamma_i T_i N \vec{u}_i \cdot \vec{n}_{target} \tag{7}$$

Electron sheath heat transmission coefficient is fixed to 4.5 whereas the ion one is fixed to 2.5 which are typical value for these quantities. Radial boundary conditions on the last flux surface are Neumanns one for all the fields (ie $\partial_{\perp}(\cdot) = 0$).

This model (equations + boundary conditions) allows the description of two principal instability mechanisms in the edge plasma: electrostatic interchange instability (driven by the opposite sign of ∇P and ∇B on low field side of the tokamak leading to a rayleigh taylor like instability) and electrostatic resistive drift waves mechanism (driven by the presence of ∇P alone) [15, 20].

1.2. Analytical magnetic geometries

In TOKAM3X, the magnetic equilibrium is not self consistently computed with the plasma equilibrium but externally imposed. This approximation is justified by the probable weak impact of the edge plasma current on the magnetic equilibrium. As a first step, this study aims to discuss the impact of triangularity alone (without adding Shafranov shift or elongation) on the edge plasma. Necessarily, it implies that the magnetic equilibria used are idealized and do not satisfy Grad-Shafranov equation. This kind of study will enable to disentangle effects of pure triangularity from effects of Shafranov shifts or elongation if we suppose a weak coupling between them. Practically, the shapes of the flux surfaces of these magnetic equilibria in polar coordinates (r, θ) are defined as follow [18, 19, 21]:

$$\begin{cases} R = R_0 + r\cos(\theta + sin^{-1}(\delta)\sin(\theta)) \\ Z = r\sin(\theta) \end{cases} \tag{8}$$

where R_0 is the major radius (radial position of the center of the plasma) and δ is the triangularity scanned for −0.5, −0.3, 0.0, +0.3 and 0.5. This formula was chosen for its simplicity and also because it is widely used for the determination of elongation and triangularity of D-shaped plasmas [18, 19, 21]. 2D maps of these magnetic equilibria are shown in figure 1. Moreover, one of the expected benefit of a hypothetical negative triangularity reactor is to increase the plasma wetted area by increasing the radial position of the targets [3]. Thus, in our scan, we have chosen to test the effects of this feature (in addition with the effect of 'pure' triangularity) by putting an infinitely thin poloidal limiter in the bottom position of each triangularity simulation without changing the aspect ratio in all the simulations. Hence, all the effects exposed in this contribution are the result of the addition of both 'pure' triangularity and increase of limiter surface. The table 1 resumes the modifications of the limiter radial position as a percentage of change with the circular test case.

1.3. Numerical setup

In all these simulations, the distance from the center of the plasma to the separatrix at midplane r_{sep} of the simulated plasma is equal to $256\rho_L$, and the aspect ratio is fixed to 3.4. Both the edge closed field lines region (CFR) and the

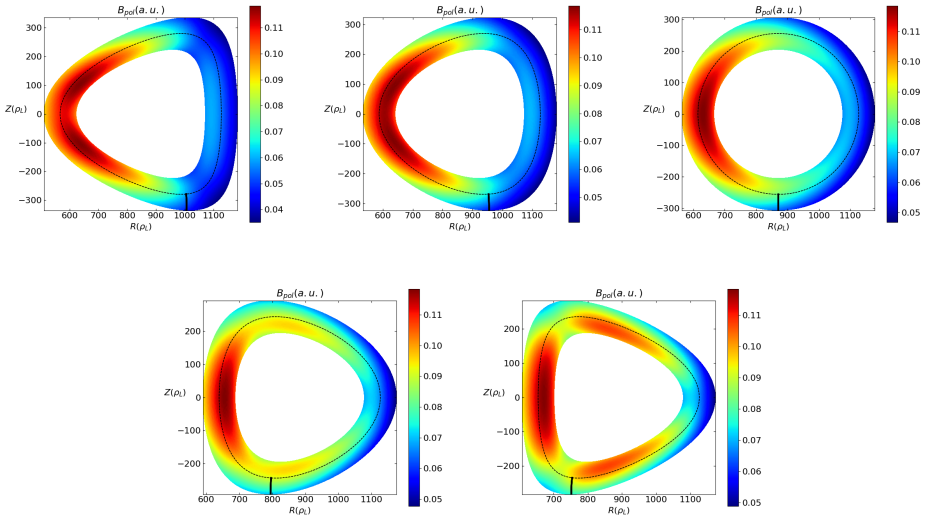

Figure 1: From top left to bottom right, 2D maps of poloidal magnetic field for $\delta = -0.5$, -0.3, 0.0, $+0.3$ and $+0.5$ triangular simulations. The black thick line represents the position of the limiter and the dashed line the separatrix. The choice to put the limiter at the bottom position while the aspect ratio remains constant is driven by the ambition to investigate both the effects of 'pure' triangularity and larger R_{target}, the latter being one of the expected benefit of a negative triangularity reactor by increasing plasma wetted area.

scrape-off layer (SOL) are simulated from $r = 0.8r_{sep}$ to $r = 1.2r_{sep}$. The safety factor q is fixed from 3 at the inner boundary to 6 at the last flux surface with a radial parabolic behavior. The sources of particles and energy have a half gaussian shape in the radial direction at the inner boundary and are poloidally and toroidally symmetric to model the influx of particles and energies reaching the edge plasma from the core. In all the simulations the volumic sources S_N and $S_{E_{e,i}}$ are identical leading to the injection of the same amount of particles and energy $\iint S_{N,E_{e,i}} d^2S_{inner\ boundary}$ as the inner surface is not modified with triangularity in our choice (8). The grid resolution used is 64 x 512 x 64 in radial r, poloidal θ and toroidal ϕ direction respectively. Thus, in terms of Larmor radius ρ_L, the average size of a mesh element is $1.6\rho_L$ x $3.1\rho_L$ x $42.7\rho_L$ in r, θ and ϕ direction respectively. All these simulations are run until quasi-stationary state is reached, i.e. the time average of total number of N, E_e and E_i do not vary on time scales longer than characteristic turbulent time scale. Once this quasi-stationnary state is reached, the statistics are made on a time sample equal to $10^5 T_C >>$ typical turbulence time scale of these TOKAM3X simulations $\sim 10^3 T_C$ where T_C is the ionic

Triangularity δ	-0.5	-0.3	0.3	0.5
Limiter radial position	+15%	+9.5%	−9.5%	−15%

Table 1: Table of the differences between the limiter radial position of all the triangularity cases simulated. The changes are expressed as a percentage of variation with respect to the circular case.

cyclotronic frequency.

2. Results

In this section, the effect of triangularity on time and toroidal averaged radial profiles at low field side midplane (section 2.1) and on turbulence characteristics (section 2.2) are discussed.

2.1. Impact of triangularity on the plasma equilibrium

Low Field Side MidPlane (LFS MP) radial profiles of density and electron temperature averaged on time and toroidal direction are represented in figure 2.

Figures 2a and 2b show that these profiles are less impacted in the CFR in comparison with the SOL. Concerning density, a global reduction along with a steepening of the averaged profiles from positive to negative triangularity simulations is visible in both CFR and the SOL. For electron temperature, no clear trend is perceptible in the CFR whereas a reduction and a steepening of the averaged profiles from $\delta > 0$ to $\delta < 0$ are observed in the SOL.

In order to quantify the most significative effect of triangularity on these profiles, i.e the steepening of average gradients in the SOL for both N and T_e, an exponential fit on the SOL radial profiles is performed following the formula:

$$F_{LFSMP}(r_{LFSmp}) = F_0 exp\Big(-\frac{r_{LFSmp} - r^{sep}_{LFSmp}}{L_F}\Big)$$

where $F = \{N, T_e\}$, F_0 represents the value of the corresponding field at the separatrix and L_F is the field decay length in the SOL at LFS MP. For each fields, these fitting parameters are resumed in table 2.

For the density, the decay length in the SOL L_N is reduced of 11% (resp. 22%) for the $\delta = -0.3$ simulation (resp. $\delta = -0.5$) in comparison with the circular case. For the positive triangularity cases, the effect has similar importance with respectively an increase of 14% (resp. 25%) of L_N for the $\delta = 0.3$ simulation (resp. $\delta = 0.5$).

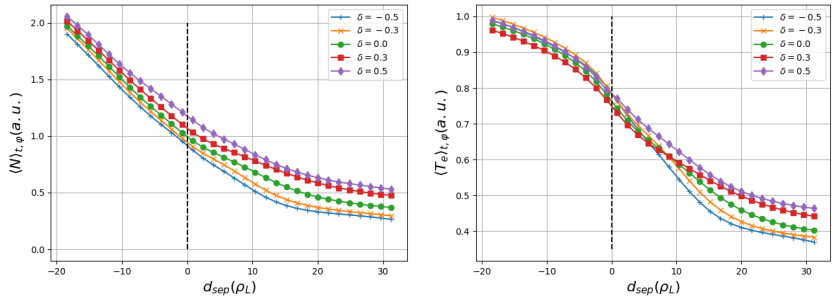

(a) (b)

Figure 2: Low Field Side Midplane (LFS MP) profiles of average on time and toroidal position of a) Density and b) Electron Temperature for different negative triangularities values (−0.5 +, −0.3 ×, 0.0 •, +0.3 ■, +0.5 ⧫). The dashed line represents the position of the separatrix which defines the frontier between the edge closed field lines region (CFR) on its left and the scrape-off layer (SOL) open field lines region on its right. For both density and electron temperature, the impact of triangularity is weaker in the edge closed field lines region compared to the SOL. From positive to negative triangularity simulations, averaged density is reduced and steepened in both the edge closed field lines region and the SOL. Average electron temperature radial profiles are also steepened in the SOL from $\delta > 0$ to $\delta < 0$ but no clear trend is visible in the edge closed field lines region. The steepening in the SOL of both average density and electron temperature gradients are measured with an exponential fit and the values of the characteristic decay lengths L_N and L_{T_e} are resumed in table 2.

For electron temperature, the effect of positive and negative triangularity on electron temperature decay length L_{T_e} is more asymmetric in comparison with the case of L_N. Indeed, whereas the $\delta = -0.3$ simulation and the $\delta = -0.5$ lead respectively to a reduction of 23% and 32% of the electron temperature decay length L_{T_e}, the $\delta = +0.3$ simulation and the $\delta = +0.5$ lead respectively to an increase of 14% and 20% of L_{T_e} in comparison with the circular case.

A quantitative comparison with experimental and other numerical scans of triangularity does not make sense as this scan is not realised in the same conditions. However, a qualitative comparison with the trends obtained in our scan is relevant to identify if the physical mechanisms included in these TOKAM3X simulations are sufficient to find the experimental trends. In the SOL, the reduction of the decay lengths at LFS MP from positive to negative triangularity values has also been identified recently by both the GBS 3D fluid turbulent code and in TCV experiments [6, 7]. In the CFR, studies on TCV [4, 5, 10] and DIII-D [2] revealed an increase of density and electron temperature along with greater average gradients from positive to negative triangularity. These observations are not in agreement

δ	-0.5	-0.3	0.0	0.3	0.5
L_N (ρ_L), %	$22\rho_L$, −22%	$25\rho_L$, −11%	$28\rho_L$	$32\rho_L$, +14%	$36\rho_L$, +25%
R^2_N	0.78	0.92	0.85	0.68	0.78
L_{T_e}(ρ_L), %	$30\rho_L$, −32%	$34\rho_L$, −23%	$44\rho_L$	$50\rho_L$, +14%	$53\rho_L$, +20%
$R^2_{T_e}$	0.86	0.92	0.72	0.77	0.66

Table 2: Table of density and electron temperature decay lengths at Low field side midplane in the scrape-off layer. The trend for both density and electron temperature decay length is to decrease from positive to negative triangularity simulations. The effect of triangularity is more asymmetric for electron temperature decay lengths in comparison with density ones. Correlation coefficients R^2 are given to quantify the quality of the exponential fits.

with what is observed in our scan on both density and electron temperatures radial profiles in this region.

Concerning the heat flux distribution on the limiter targets, triangularity has also an influence. The parallel to **B** heat flux reaching the limiter target can be written as follows:

$$q_{||} = \Gamma^t(\gamma_e T_e^t + \gamma_i T_i^t)$$

where Γ is the ion parallel to **B** particle flux, F^t the value of a certain field (N,T_e,T_i,Γ) at the target position and $\gamma_{e/i}$ the electron/ion sheath heat transmission coefficients fixed to $\gamma_e = 4.5$ and $\gamma_i = 2.5$ [16]. The inner and outer target radial profiles of the parallel to **B** heat flux averaged in time and toroidal position are represented in figure 3a and 3b. These profiles are remapped to LFS MP of the circular simulation to be comparable.

An exponential fit is performed to capture the behavior of these profiles following the formula:

$$q_{||}(r_{LFSmp}) = q_{||_0} exp\Big(-\frac{r_{LFSmp} - r^{sep}_{LFSmp}}{\lambda_q}\Big) \tag{9}$$

where $q_{||_0}$ is the peak value of the parallel to **B** heat flux and λ_q the SOL power fall-off length remapped at LFS mp. The table 3 resumes these principal characteristics for inner and outer target. On both inner and outer targets, a clear reduction of λ_q and q_0 from positive triangularity simulations to negative ones can be observed. The conservation of the energy is assured by the increase of the limiter surface from positive to negative triangularity simulations (see section 1.2 and [3]). It is interesting to notice that the decrease of λ_q with negative triangular-

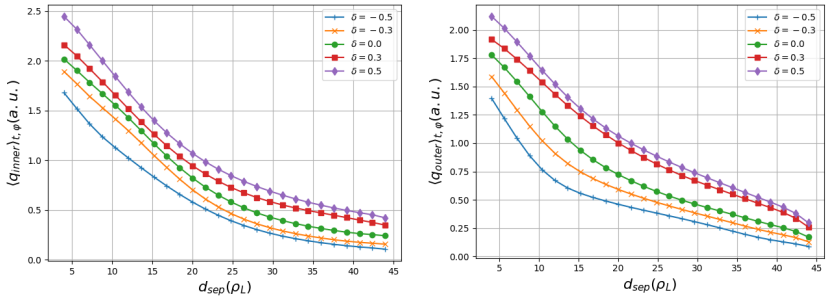

(a) (b)

Figure 3: a) Inner and b) outer targets radial profiles for different triangularities values (−0.5 +, −0.3 ×, 0.0 •, +0.3 ■, +0.5 ⧫). The profiles are remapped to LFS midplane of circular simulation for relevant comparison. On both inner and outer targets, the peak value of the heat flux q_0 and the SOL power fall-off length remapped at LFS MP λ_q are decreased from positive to negative triangularity values. The detailed values are resumed in table 3. The conservation of the energy is assured by the increase of the limiter surface from positive to negative triangularity simulations.

ity potentially counteracts the expected beneficial effect of negative triangularity leading to a larger R_{target}.

δ	-0.5	-0.3	0.0	0.3	0.5
Peak q_0 (a.u.)	(1.7, 1.4)	(1.9, 1.6)	(2.0, 1.8)	(2.2, 1.9)	(2.5, 2.2)
$\lambda_q(\rho_L)$	(23, 18)	(27, 23)	(30, 28)	(33, 37)	(35, 41)
R^2	(0.98, 0.72)	(0.78, 0.80)	(0.83, 0.87)	(0.73, 0.89)	(0.77, 0.85)
$\frac{\lambda_q^{in}}{\lambda_q^{out}}$	1.28	1.17	1.07	0.89	0.85

Table 3: Table of principal characteristics of heat fluxes entering on (inner, outer) targets. Both q_0 and λ_q at inner and outer targets are reduced from positive to negative triangularity values. The increase of limiter surface from $\delta > 0$ to $\delta < 0$ assures the conservation of energy in all the simulations. Correlation coefficients R^2 are given to quantify the quality of the exponential fits.

These modifications in the time averaged LFS MP profiles and target profiles are directly linked to changes in turbulence as turbulence plays a dominant role in the transport of both particles and energy in TOKAM3X simulations. The impact of triangularity on turbulence is addressed now in the following section.

2.2. Impact of triangularity on turbulence

Figure 4 shows 2D snapshots at a given time and toroidal position of the relative level of density fluctuations $\frac{N-\langle N\rangle_{t,\varphi}}{\langle N\rangle_{t,\varphi}}$ of each simulations. From these snapshots, two principal features seem clear: first, the classical ballooning feature of turbulence seems to be not modified by the addition of triangularity. Quantitatively, the ballooning of turbulence in the different simulations is compared by computing a poloidal profile of the relative level of density fluctuations $\frac{\sigma_N}{\langle N\rangle_{t,\varphi}}$ averaged on time and toroidally at a certain radial position. Figure 5a shows such profile at $r = 1.05 r_{separatrix}$ in the SOL. It is clear from this plot that for all the triangularity cases, the maximum of turbulence remains close to the LFS MP while its intensity decreases when we approach the high field side. This observation is also valid for the absolute fluctuations amplitude (not shown here) proving that the difference in average density is not the only factor responsible for this effect. The trend is identical for all the other radial positions and fields.

The second observation concerns the radial dependence of the relative level of density fluctuations that seems to be higher in the SOL compared to the CFR for all the triangularity simulations. This observation is confirmed by the computation of the relative level of density $\sigma_N/\langle N\rangle_{t,\varphi}$ and electron temperature fluctuations $\sigma_{T_e}/\langle T_e\rangle_{t,\varphi}$ averaged on time and toroidally at LFS MP. These latter are represented on figures 5b and 5c.

In the SOL, both $\sigma_N/\langle N\rangle_{t,\varphi}$ and $\sigma_{T_e}/\langle T_e\rangle_{t,\varphi}$ are enhanced (resp. reduced) by negative (resp. positive) triangularity whereas in the CFR, no global trend is visible. In addition, the impact of triangularity on the relative level of density fluctuations is greater than its impact on the relative level of electron temperature fluctuations.

Experimentally, independent studies have been carried out recently on TCV [4, 5, 24] and DIII-D [1, 2] where the radial dependencies of $\sigma_N/\langle N\rangle_t$ and $\sigma_{T_e}/\langle T_e\rangle_t$ until the edge closed field lines region in negative and positive triangularity discharges have been measured. The TCV studies report a reduction of both $\sigma_N/\langle N\rangle_t$ and $\sigma_{T_e}/\langle T_e\rangle_t$ in this region for the negative triangularity discharge in comparison with the positive one. The difference increases from the core to the edge closed field lines region. In DIII-D, the qualitative trend is identical but is quantitatively less important than in the TCV measurements. In comparison, our scan does not reveal either significative reduction of $\sigma_N/\langle N\rangle_t$ and $\sigma_{T_e}/\langle T_e\rangle_t$ in this region. As different experiments with different setups (different ways of heating of the plasma, different plasma characteristics, ...) have come to this same conclusion revealing its robustness, it is possible that some key physical phenomena

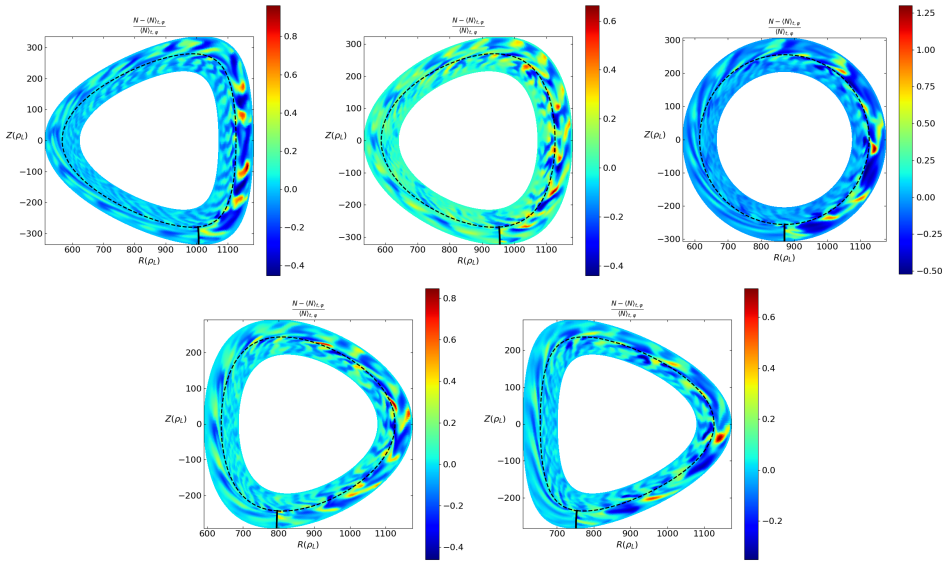

Figure 4: From top left to bottom right, 2D Snapshots of relative level of density fluctuations $\frac{N-\langle N\rangle_{t,\phi}}{\langle N\rangle_{t,\phi}}$ for $\delta = -0.5, -0.3, 0.0, +0.3$ and $+0.5$ triangular simulations given at an arbitrary time and toroidal position. The black thick line represents the position of the limiter and the dashed line the separatrix. These figures reveal that the classical ballooning feature of turbulence seems to be not affected by triangularity and that the turbulence relative level is higher in the SOL compared to the edge closed field lines CFR region.

in the passage from $\delta > 0$ to $\delta < 0$ is missing in the TOKAM3X physical model used to simulate the edge closed field lines region. In other words, it is possible that turbulence developed from electrostatic interchange and electrostatic resistive drift waves is not sufficient to reproduce the effects of triangularity on the level of fluctuations of both T_e and N in the plasma located in the edge closed field lines region. Another possibility is linked to the abnormal high values of collisionality used in these simulations for numerical reasons. Indeed, experiments on TCV have shown that the relative confinement improvement between positive and negative δ was found to reduce for increasing collisionality [22].

3. Concluding remarks and discussion

A scan in triangularity has been performed in full 3D fluid turbulence simulations with the TOKAM3X code in a bottom limited configuration encompassing the edge last closed field lines region (CFR) and the scrape-off layer (SOL).

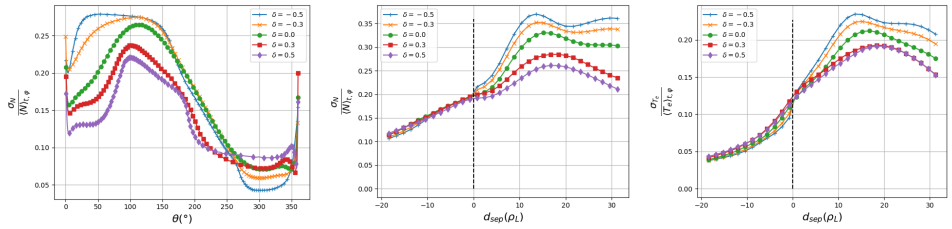

(a) (b) (c)

Figure 5: (a) Poloidal profile of the relative level of density fluctuations $\sigma_N/\langle N\rangle_{t,\varphi}$ at $r = 1.05 r_{sep}$ in the SOL averaged in time and toroidal direction. θ is the angle between a vertical line passing by the center of the plasma and the poloidal location. Thus, 0° is the position of the limiter, 90° the position of the low field side midplane, 180° the position of the top, 270° the high field side midplane position. The latter shows that ballooning character of turbulence is not affected by triangularity with a maximum of turbulence level at LFS MP. (b),(c) Low Field Side Midplane radial profiles of relative level of fluctuations of (b) density $\sigma_N/\langle N\rangle_{t,\varphi}$ and (c) electron temperature $\sigma_{T_e}/\langle T_e\rangle_{t,\varphi}$ averaged on time and toroidal direction for different negative triangularities values (-0.5 +, -0.3 ×, 0.0 •, $+0.3$ ■, $+0.5$ ⧫). The dashed line represents the position of the separatrix which defines the frontier between the edge closed field lines region on its left and the SOL open field lines region on its right. The effect of triangularity is higher in the SOL where both $\sigma_N/\langle N\rangle_{t,\varphi}$ and $\sigma_{T_e}/\langle T_e\rangle_{t,\varphi}$ are enhanced (resp. reduced) by negative (resp. positive) triangularity. In the edge closed field lines region, no clear trend is visible. We notice also that the impact of triangularity on the relative level of density fluctuations is greater than its impact on the relative level of electron temperature fluctuations.

Concerning the plasma equilibrium, a global reduction along with a steepening of the averaged profiles of the density from positive to negative triangularity simulations is shown in both the CFR and the SOL. For the electron temperature, if no clear trend is visible in the CFR, simulations show a reduction along with a steepening of the averaged profiles of T_e from $\delta > 0$ to $\delta < 0$ in the SOL. This corresponds to a reduction of the density and the electron temperature decay lengths for negative triangularity. With respect to results of the literature, present results are not in agreement in the CFR with average radial profiles measured on TCV [4, 5, 10, 24] and DIII-D [2]. However in the SOL, they are consistent with the results measured in TCV and from GBS simulations [6, 7]. On the limiter targets, the distribution of the heat flux is also impacted by triangularity. Indeed, both the peak value q_0 of the heat flux and the SOL power fall-off length λ_q are reduced on the inner and outer targets with negative triangularity. The conservation of the energy is assured by the increase of the limiter radial position from positive to negative triangularity simulations in the current configuration. It is notable that the reduction of λ_q^{out} potentially partly counteracts the benefit of negative triangu-

larity leading to a larger R_{target}.

Concerning the turbulence characteristics, no impact of triangularity on the ballooning feature is observed. In the SOL, the relative level of fluctuations is increased from positive to negative triangularity simulations for both density and electron temperature fields. In contrast, no clear trend is identifiable in the CFR. This enhancement of turbulence fluctuations in the SOL differs from TCV [4, 5, 24] and DIII-D [1, 2] measurements which show on the contrary a large reduction of the density and electron temperature relative level of fluctuations with negative triangularity in the edge closed field lines region.

No clear conclusion can be however drawn from this preliminary study concerning the impact of triangularity on the turbulent transport, which has not been investigated here. Turbulent transport depends indeed not only on the amplitude of the density fluctuations but also on the fluctuations of the electric potential, of the phase between potential and density fluctuations, as well as of the size of the turbulent structures since the smaller they are, the larger the poloidal gradient and therefore the larger the related radial EXB velocities are. It is also noticeable that triangularity also impacts the poloidal symmetry of the problem, so that turbulence properties might not be impacted uniformly at all points in the poloidal direction. Therefore, present results shwowing only the enhancement of density fluctuations in the SOL at the LFS midplane cannot be conclusive regarding the turbulent transport. Further studies on turbulent transport would be needed in the whole domain to establish an exhaustive picture of the phenomenology at play. In addition, in the current configuration the triangularity changes the geometry (size of the limiter) which has a direct impact on the decay length of the density. One of the points highlighted by this work is to show that the change in triangularity impacts many simulation control parameters, as in the experiments, and that the analysis of its impact alone on the dynamics of the plasma is not obvious in this configuration. Simulations with a HFS localized limiter to control its geometry during the change of triangularity are in progress to investigate this issue.

Finally, the limitations of the TOKAM3X model can also have a role in the discrepancies observed with the experiments. On this point, recent gyro-kinetic simulations (GS2, GENE, LORB5 [8, 9, 10, 22, 24]) have been able to reproduce qualitatively the effects of triangularity on electron heat transport in the edge closed field lines region. In particular, these simulations have shown in particular the importance of the treatment of TEM to reproduce the effects of negative triangularity in this region.

Acknowledgements

This work has been carried out within the framework of the EUROfusion Consortium and has received funding from the Euratom research and training programme 2014-2018 and 2019-2020 under grant agreement No 633053. The views and opinions expressed herein do not necessarily reect those of the European Commission. This work has been carried out also thanks to the support of the A*MIDEX project (ANR-11-IDEX-0001 02) funded by the Investissements dAvenir French Government program, managed by the French National Research Agency (ANR). This work was granted access to the HPC resources of IDRIS under the allocations A0030506912 & A0050506912 made by GENCI, of Aix-Marseille University, nanced by the project Equip@Meso (ANR-10-EQPX-29 01), and of the EUROfusion High Performance Computer (Marconi-Fusion) under the project HEAT.

[1] M.E. Austin and al, *PRL* **122**, 115001 (2019).

[2] A. Marinoni and al., *Physics of Plasmas* **26**, 042515 (2019).

[3] M. Kikuchi and al., *Nucl. Fusion* **59**(6) 056017 (2019).

[4] Z. Huang and al., *Plasma Phys. Control. Fusion* **61** 014021 (2019).

[5] M. Fontana and al., *Nucl. Fusion* **58** 024002 (2018).

[6] F. Riva and al., *Plasma Phys. Control. Fusion* **59** 035001 (2017).

[7] F.Riva and al., *Physics of Plasmas* **27**, 012301 (2020).

[8] G. Merlo and al., *Plasma Phys. Control. Fusion* **57** 054010 (2015).

[9] A Marinoni and al., *Plasma Phys. Control. Fusion* **51** 055016 (2009)

[10] Y. Camenen and al., *Plasma Phys. Control. Fusion* **47** 1971 (2005).

[11] M. Faitsch and al., *Plasma Phys.Controlled Fusion* **60**, 045010 (2018)

[12] P. Tamain and al., *J. Computat. Phys.* **321**, 606 (2016).

[13] C. Baudoin and al., *Contributions to Plasma Physics*, **58**, 484489 (2018).

[14] S. I. Braginskii, Transport processes in a plasma, *M.A. Leontovich (Ed.), Reviews in Plasma Physics, vol. 1, Consultants Bureau, New York* (1965).

[15] A. Hasegawa and K. Mima, *Physical Review Letter* **39**, 205 (1977).

[16] P. Stangeby, The Plasma Boundary of Magnetic Fusion Devices, *Plasma Physics Series edited by Taylor and Francis group*(2000).

[17] D.M. Fan and al., *Contributions to Plasma Physics* **58** 490496 (2018).

[18] R. L. Miller and al., *Physics of Plasmas* **5**, 973 (1998).

[19] J.-M. Moret and al., *Physical Review Letters* **79, 11**, 2057-2060 (1997).

[20] R. J. Goldstone, Introduction to Plasma Physics, *Institute of Physics Publishing Bristol and Philadelphia* (1995).

[21] A. M. M. Todd and al., *Nucl. Fusion* **19**, 743 (1979).

[22] Y. Camenen and al., *Nucl. Fusion* **47**, 510 (2007).

[23] W. Han and al., 'Exploring the Dependence of Edge/SOL Turbulence Suppression of First-wall Interaction in Negative Triangularity Plasmas on TCV', Abstract submitted for the DPP20 Meeting of The American Physical Society (2020)

[24] M. Fontana and al., *Nucl. Fusion*, **60** 016006 (2020).